# Effects of inter-vanadium distance and $A$-site magnetism in $AV_2O_4$ ($A$ = Cd, Mg, Zn) spinels near the itinerant electron limit

A. Kiswandhi,[1,2,*] J. Ma,[3] J. S. Brooks,[1,2] and H. D. Zhou[1,4]

[1]*National High Magnetic Field Laboratory, Florida State University, Tallahassee, Florida 32306-4005, USA*

[2]*Department of Physics, Florida State University, Tallahassee, Florida 32306-3016, USA*

[3]*Quantum Condensed Matter Division, Oak Ridge National Laboratory, Oak Ridge, Tennessee 37831, USA*

[4]*Department of Physics and Astronomy, University of Tennessee, Knoxville, Tennessee 37996-1200, USA*

(Received 25 July 2014; revised manuscript received 9 October 2014; published 30 October 2014)

We present temperature dependent powder x-ray diffraction measurements of the spinel $AV_2O_4$ ($A$ = Cd, Mg, Zn, and $Mn_{1-x}Co_xV_2O_4$). The result shows that even though the V-V distance is an important governing parameter, the $A$-site magnetism also has a significant effect on the physical properties of $AV_2O_4$. This is demonstrated by comparing the structural and transport properties of nonmagnetic $A$-site ions $AV_2O_4$ ($A$ = Cd, Mg, Zn) with the magnetic $A$-site ion substitutional sequence $Mn_{1-x}Co_xV_2O_4$.

DOI: 10.1103/PhysRevB.90.155132 PACS number(s): 72.80.Ga, 71.30.+h, 75.50.Dd, 61.05.cp

## I. INTRODUCTION

The spinel system $AV_2O_4$, ($A$ = Cd, Mg, Zn, Mn, Fe, and Co) has received considerable attention due to its physical properties resulting from the interplay among the spin-lattice coupling from its localized 3$d$ electrons, orbital degrees of freedom, and its geometrically frustrated structure [1]. Many of the available $AV_2O_4$ studies focus on (1) the effect of magnetic/nonmagnetic $A$-site ions, (2) the effect of orbitally active/inactive ions on the $A$ and/or $B$ site, and (3) the lattice size effect. The latter treats the $A$-site ion as a tuning parameter to influence the inter-vanadium distance $R_{V\text{-}V}$ that is believed to control most of the properties of the system [2,3]. In $AB_2X_4$ ($X$ = O, S, Se) spinels, direct $B$-$B$ interactions are possible and their strength depends on the $B$-$B$ distance and anion shielding if the $B$-site $t_{2g}$ orbitals are half filled or less (and degenerate) [4]. This condition is realized in vanadium spinels whose electron configuration of the $V^{3+}$ is $t_{2g}^2 e_g^0$. Studies have shown that $R_{V\text{-}V}$ is a critical parameter that controls the physical properties of the $AV_2O_4$ spinel [5].

In the high pressure study by Kismarahardja *et al.*, it was demonstrated that an insulator to metal transition can be induced in $CoV_2O_4$ at $P = 6$ GPa [6]. Using an assumption that the compressibility in the $AV_2O_4$ system is similar, it can be estimated that at 6 GPa the value of $R_{V\text{-}V}$ is less than its critical value of 2.94 Å, below which a metallic conductivity should be observed. Even though there is no high pressure structural study data available for $CoV_2O_4$, a recent theoretical study by Kaur *et al.* [7] showed that by lowering the crystal symmetry to tetragonal yields a greater total energy, compared to that of the cubic structure, and hence the system most likely remains cubic even at the high pressure regime where metallic conduction is observed. This implies that the value of $R_{V\text{-}V}$ does not abruptly change due to a structural transformation. (This study also considered the possibility of cation inversion and it was found that such inversion is energetically unfavorable.)

Chemical pressure/chemical substitution of the $A^{2+}$ ion also provides an alternative way of varying $R_{V\text{-}V}$, and our previous study on $Mn_{1-x}Co_xV_2O_4$ showed that the effect of physical pressure and chemical substitution are qualitatively similar, suggesting a dominant $V^{3+}$-$V^{3+}$ interaction [8]. The importance of $R_{V\text{-}V}$ is also apparent in the transport studies of $AV_2O_4$ where it has been shown that (1) the activation energy decreases with decreasing $R_{V\text{-}V}$ and (2) $MgV_2O_4$ and $ZnV_2O_4$ have similar activation energies due to similar values of $R_{V\text{-}V}$ [9].

In this paper, the lattice size ($R_{V\text{-}V}$) effect in the $AV_2O_4$ system with nonmagnetic $A$-site ions ($A$ = Cd, Mg, and Zn) is reinvestigated and compared to that of $Mn_{1-x}Co_xV_2O_4$ ($x$ = 0.2, 0.4, 0.6) with magnetic $A$-site ions. $Mn_{1-x}Co_xV_2O_4$ is ideal since its $R_{V\text{-}V}$ decreases continuously with $x$ between $MnV_2O_4$ and $CoV_2O_4$, in the proximity of $R_{V\text{-}V}$ for $MgV_2O_4$ and $ZnV_2O_4$. In addition, both $Mn^{2+}$ and $Co^{2+}$ in the tetrahedral environment are orbitally inactive. Therefore, one can study exclusively the influence of the $A$-site ion magnetism on the physical properties without complications from orbital degrees of freedom.

## II. EXPERIMENTAL

Single crystals of $Mn_{1-x}Co_xV_2O_4$ and $MgV_2O_4$ were grown using the traveling-solvent floating-zone technique (TSFZ) in an optical furnace following the procedure described in our previous publication [8]. For $MgV_2O_4$, an appropriate mixture of MgO and $V_2O_3$ were ground together and calcined in a 10% $H_2$/Ar atmosphere at 1000 °C for 40 h in order to prepare the feed and seed rods for TSFZ growth. A small amount of MgO was added in preparing the rods in order to compensate for the loss during synthesis due to evaporation. The growth was carried out in an Ar atmosphere with the feed and seed rods rotating in opposite directions at 25 rpm with the growth rate of 20 mm/h. For consistency, the same crystals of $Mn_{1-x}Co_xV_2O_4$ used in Ref. [8] were used here for structural measurements.

Polycrystalline samples of $AV_2O_4$ ($A$ = Cd, Zn) were prepared using a solid state reaction method in evacuated quartz tubes at 800 °C using graphite crucibles. The crystals were ground into powder in order to perform the powder x-ray diffraction (XRD) measurement. The temperature dependent

*kiswandhi@magnet.fsu.edu

 

XRD measurements were performed using a HUBER Imaging Plate Guinier Camera 670 with Ge monochromatized Cu $K_{\alpha 1}$ radiation. The measurement was done with 20 K steps at high temperature and 1 K steps in the vicinity of structural transition temperature $T_S$. The resulting XRD patterns were analyzed with a Rietveld refinement method by using GSAS [10] and EXPGUI [11] software packages.

## III. RESULTS AND DISCUSSION

The temperature dependent lattice parameters for $A = $ Cd, Mg, and Zn are presented in Fig. 1, while Fig. 2 shows the temperature dependencies of the lattice parameters for the $Mn_{1-x}Co_xV_2O_4$ system. The result confirms the high temperature cubic phase with $Fd\bar{3}m$ symmetry. The lattice parameter of the cubic phase was fit to a quadratic function $a_{\rm fit} = AT^2 + a_0$. The low temperature tetragonal phase was refined using $I4_1/amd$ symmetry with $c_t < a_t\sqrt{2}$. The relative change of the lattice parameter $a$ was calculated as $\delta a(T) = [a(T) - a_{\rm fit}]/a_{\rm fit}$ (in the tetragonal phase $a = a_t\sqrt{2}$). Likewise, the relative change in the lattice parameter $c$ was calculated as $\delta c(T) = [c(T) - a_{\rm fit}]/a_{\rm fit}$ ($c = c_t$ in the tetragonal phase). The resulting structural transition temperature $T_S$ is tabulated in Table I. The $T_S$ values are consistent with previous work [12–15].

In reference to Figs. 1 and 2, it is important to note that the changes in the lattice parameters at $T_S$ are the most abrupt for the nonmagnetic $AV_2O_4$ and the $Mn_{0.8}Co_{0.2}V_2O_4$ compounds, but these changes are significantly less abrupt for $x = 0.4$ and 0.6. Indeed, there is a direct correspondence between the abruptness of the transition and phase coexistence as evidenced in the XRD patterns for $A = $ Cd, Zn, and $x = 0.2$ shown in Fig. 3 over a temperature range at $T \leqslant T_S$ at which the pattern cannot be fitted with either a single $Fd\bar{3}m$ or $I4_1/amd$ phase. These compounds show a region of phase coexistence between the cubic and tetragonal phases, which is an indication of a first order transition and consistent with the heat capacity data that show a discontinuous jump at $T_S$ [8,13,15,16]. To find the volume percentage of the tetragonal phase, a selected Bragg peak that exhibited splitting was fit with Lorentzian functions to obtain the integrated intensities of each of the split peaks. Figure 3 shows the splitting of specific peaks of the $CdV_2O_4$, $ZnV_2O_4$, and $x = 0.2$ compounds. For $CdV_2O_4$, the (400) peak is weak, so the (440) peak is used instead. The volume percentage of the tetragonal phase then can be calculated as $I_{\rm tet}/(I_{\rm tet} + I_{\rm cubic})$, shown in Fig. 4 as a function of normalized temperature, $T/T_S$. From Fig. 4, it can be seen that the region of phase coexistence spanned about 5 to 10 percent of the transition temperature, and the phase percentage as a function of normalized temperature behavior for each sample is similar, except for $MgV_2O_4$. It has been shown that the temperature range of phase coexistence in $MgV_2O_4$ is dependent on the sample growth method which influences the stoichiometry and site disorder in the sample [17]. However, this does not affect the transition temperature if one defines $T_S$ as the temperature below which the XRD pattern can no longer be fitted by a single cubic phase and not the temperature at which the phase turns 100% tetragonal. In contrast, neither $x = 0.4$ nor 0.6 show this phase coexistence, signaling weaker structural distortion that is consistent with the data shown in Fig. 2 and also heat

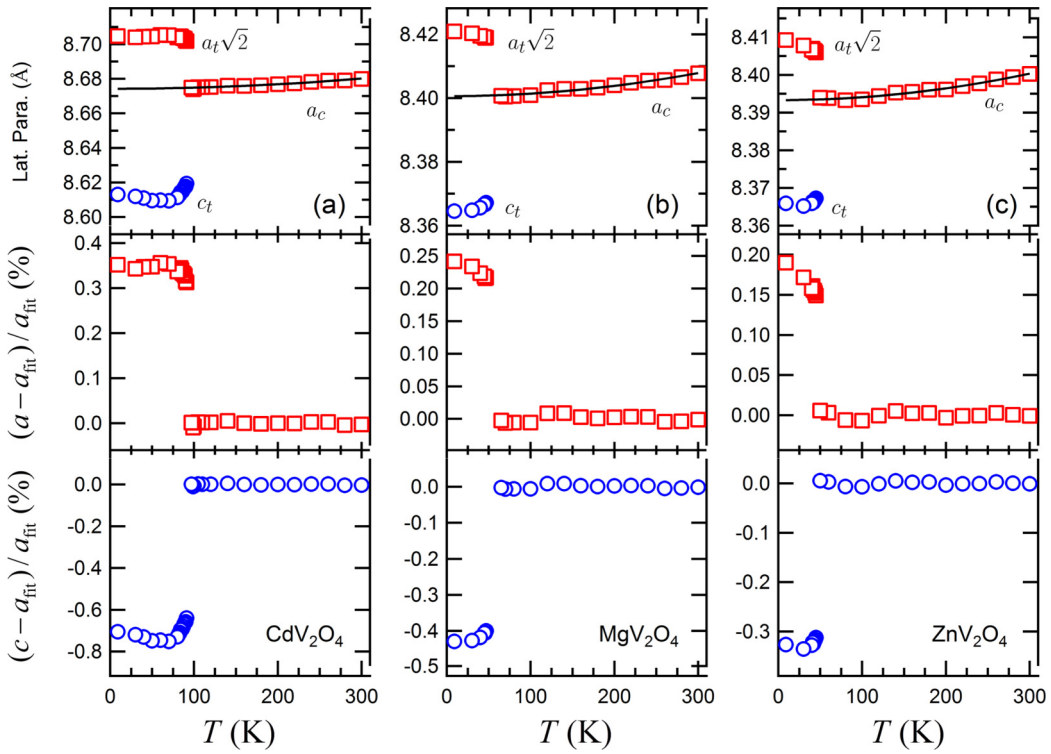


FIG. 1. (Color online) Nonmagnetic $A$-site $AV_2O_4$. Results of the Rietveld refinements showing the temperature dependencies of the lattice parameters and the fit (solid lines) to the lattice parameters of the cubic phase (top), and the percentage of the changes in the lattice parameters $a$ (center) and $c$ (bottom) for (a) $CdV_2O_4$, (b) $MgV_2O_4$, and (c) $ZnV_2O_4$.

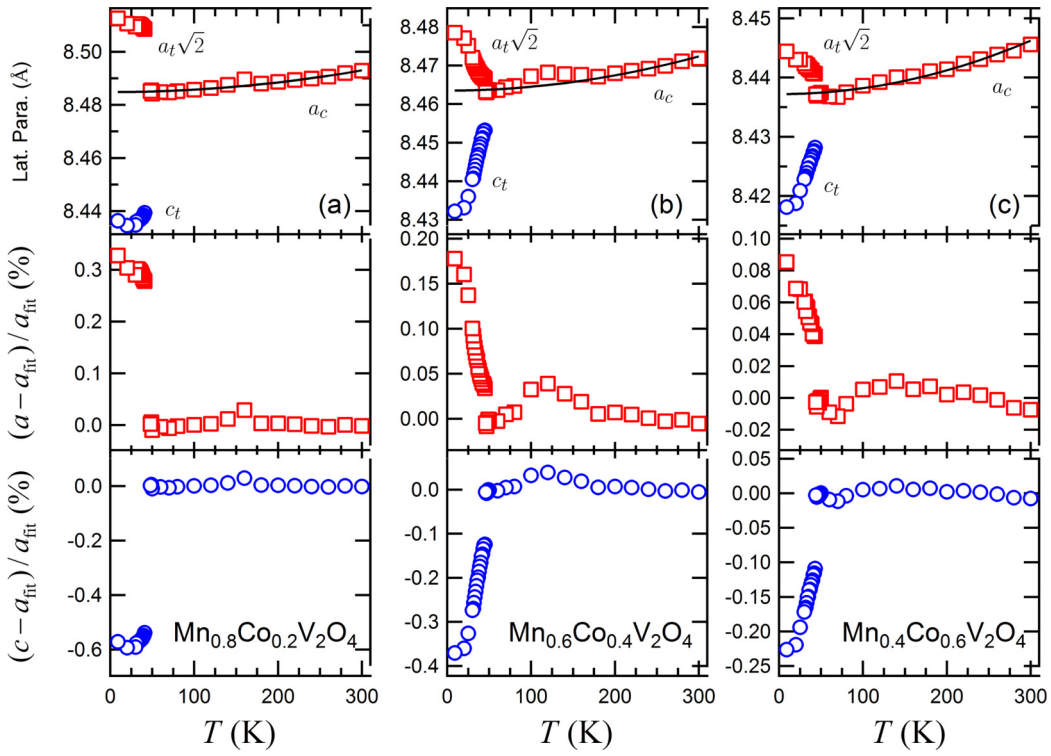


FIG. 2. (Color online) Magnetic $A$-site $Mn_{1-x}Co_xV_2O_4$. Results of the Rietveld refinements showing the temperature dependencies of the lattice parameters and the fit (solid lines) to the lattice parameters of the cubic phase (top), and the percentage of the changes in the lattice parameters $a$ (center) and $c$ (bottom) for (a) $x = 0.2$, (b) $x = 0.4$, and (c) $x = 0.6$.

capacity data where only a hump instead of a sharp peak is apparent at $T_S$ [8].

The values of the relative changes of the lattice parameters at 10 K as a function of $R_{V\text{-}V}$(300K) are summarized in Figs. 5(a) and 5(b). In $AV_2O_4$, the tetragonal distortion occurs due to the degeneracy of the $t_{2g}$ orbital of $V^{3+}$, leading to the Jahn-Teller effect. In the tetragonal distortion with very small changes in the volume, the changes in the lattice parameter can be roughly estimated as $\delta V = a^2\delta c + 2ac\delta a$. Given that $\delta V$ is small and $c \approx a$, then $\delta c = -2\delta a$. It can be seen in Figs. 5(a) and 5(b) that the ratio of relative changes, $\delta a$ to $\delta c$, is about 1:2. However, the relative changes of the tetragonal distortion progressively decreases with decreasing lattice size. It is informative to compare this to the more conventional measure of lattice distortion, which is the $c/a$ ratio [Fig. 5(c)]. The values of the $c/a$ ratio are found to be in good agreement with available references [6,12–15]. The values of $T_S$ and activation energy measured from the resistivity ($E_A$) as a function of $R_{V\text{-}V}$(300 K) are also summarized in Figs. 6(a) and 6(b).

TABLE I. Structural transition temperatures of the $AV_2O_4$ and $Mn_{1-x}Co_xV_2O_4$ spinels and the range of the phase coexistence region ($\delta T$).

| Compound | $T_S$ (K) | $\delta T$ (K) |
|---|---|---|
| $CdV_2O_4$ | 96 | 5 |
| $MnV_2O_4$ | 57 | 3 |
| $MgV_2O_4$ | 64 | 17 |
| $ZnV_2O_4$ | 49 | 4 |
| $Mn_{0.8}Co_{0.2}V_2O_4$ | 47 | 6 |
| $Mn_{0.6}Co_{0.4}V_2O_4$ | 45 | 0 |
| $Mn_{0.4}Co_{0.6}V_2O_4$ | 43 | 0 |

A main result of the present work is as follows. For all physical properties described in Figs. 5 and 6, *there are two different paths that the system follows in approaching the critical* $R_{V\text{-}V}$. One path follows Cd-Mg-Zn-Co (solid red line). For some physical properties this path also includes the Mn sample. The other path follows the Co-doping in $Mn_{1-x}Co_xV_2O_4$ (the dashed blue line). To demonstrate the difference between these two paths, we compare two samples: the Zn sample on path 1 and the $x = 0.4$ sample on path 2. These two samples have almost identical characteristics, including lattice parameter changes and $c/a$ ratio (or the magnitude of the distortion) and similar $T_S$ and $E_A$ values, *but with different* $R_{V\text{-}V}$ *values*. Another important difference in these two samples is that the Zn sample has phase coexistence around $T_S$ whereas no detectable phase coexistence is observed in the $x = 0.4$ sample. If the $x = 0.4$ sample follows path 1 then it should have larger distortion (smaller $c/a$ ratio), higher $T_S$, and higher $E_A$ due to its larger $R_{V\text{-}V}$. In addition, Fig. 6(b) also shows the activation energy is reduced for $x = 0.6$ as compared to $A =$ Fe, despite the similar value of $R_{V\text{-}V}$. The questions that then arise are why these two samples have similar physical properties but with different $R_{V\text{-}V}$ values and how two paths in approaching the critical $R_{V\text{-}V}$ emerges. *We assert that our results show that* $R_{V\text{-}V}$ *is not the only controlling factor, but that A-site magnetism plays an additional role.*

In $CdV_2O_4$, the large $T_S$ and $E_A$ can be explained by the lattice/ion size effect, due to its considerably larger size compared to that of other $AV_2O_4$ compounds. Therefore, due

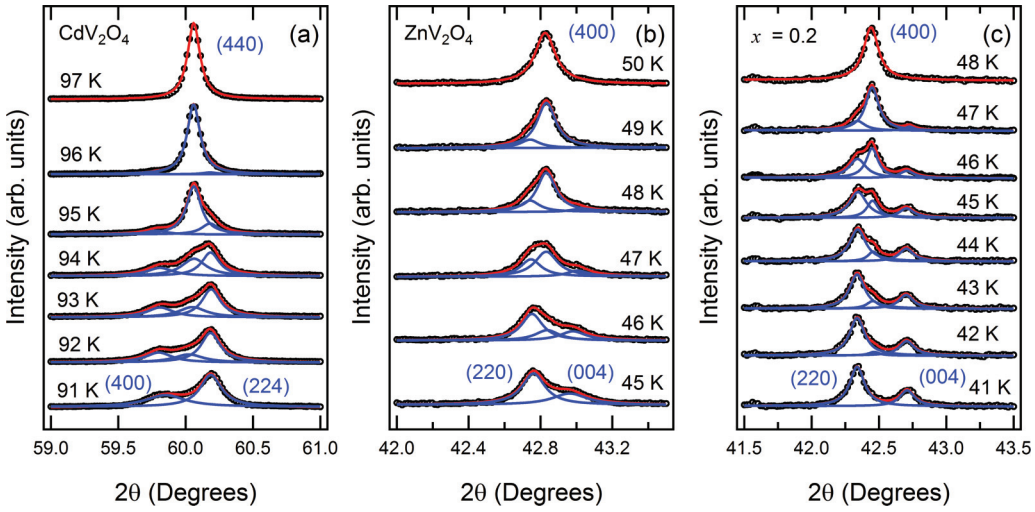


FIG. 3. (Color online) The XRD pattern of a selected peak of (a) $CdV_2O_4$ (440), (b) $ZnV_2O_4$ (400), and (c) $Mn_{0.8}Co_{0.2}V_2O_4$ (400) in the proximity of $T_S$ showing the evolution of the peak with temperature. The solid blue curves are the Lorentzian fit to the peaks.

to the large $R_{V\text{-}V}$ the electrons are more localized. In addition, Zhang *et al.* suggest that the large lattice parameter leads to a relatively softer lattice which more readily deforms [18]. This effect is also suggested by the magnitude of the tetragonal distortion in $CdV_2O_4$. In $MgV_2O_4$ with the completely empty $t_2$ orbitals on the $Mg^{2+}$ sites and $ZnV_2O_4$ with the fully occupied $t_2$ orbitals on the $Zn^{2+}$ sites, the V-V interaction still dominates. Also, owing to the similarity in $R_{V\text{-}V}$ both have a similar $E_A$. However, $ZnV_2O_4$ has a slightly smaller $R_{V\text{-}V}$ that makes it closer to the itinerant electron limit, so as a result $T_S$ decreases and the tetragonal distortion is weakened in $ZnV_2O_4$. Finally, $T_S$ is significantly suppressed in $CoV_2O_4$ where no detectable tetragonal distortion is observed down to $T = 5$ K [19]. The suppression of the structural distortion is modeled by the formation of V-V dimers that results in an alternating long and short V-V bond [9]. This bond length alternation occurs as a result of a partial electronic delocalization without the need of orbital ordering in $AV_2O_4$ and may cause a structural distortion with a net effect of $c \approx a$.

An important distinction between path 1 and path 2 is as follows. On path 1, it is understood that the activation energy decreases systematically in approaching the itinerant electron limit. However, on path 2 with $Mn_{1-x}Co_xV_2O_4$ the situation changes. From the first-principle calculations for the projected density-of-states of $FeV_2O_4$, $MnV_2O_4$, and $CoV_2O_4$ onto $t_{2g}$ and $e_g$ orbitals of Fe, Mn, Co, and V ions, the energy difference between the occupied V and Co $d$ states is the smallest, which enhances the itinerancy [19,20]. Therefore, the activation energy of the $x = 0.4$ sample with a larger $R_{V\text{-}V}$ is significantly reduced to a value comparable to that of the Zn

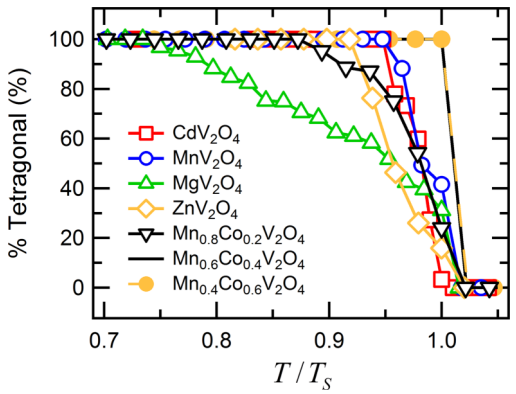


FIG. 4. (Color online) The percentage of the tetragonal phase as a function of normalized temperature $T/T_S$.

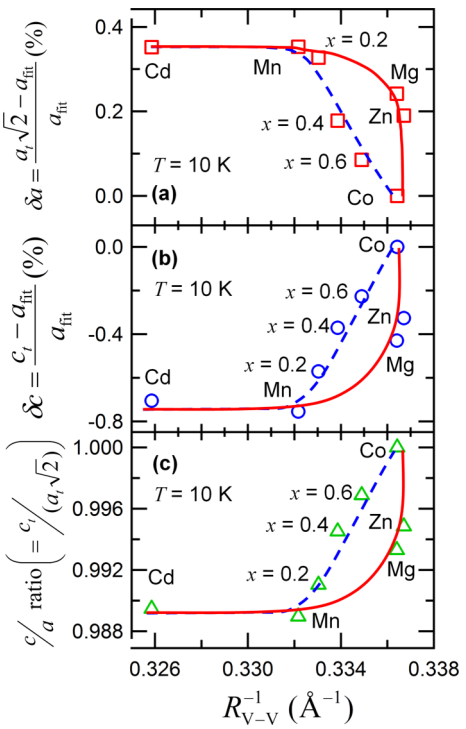


FIG. 5. (Color online) The $R_{V\text{-}V}$ dependencies (plotted as $R_{V\text{-}V}^{-1}$) of (a) the relative changes of $a$ of $AV_2O_4$, (b) the relative changes of $c$, and (c) the $c/a$ ratio. The plots show the two schematic paths of how the magnitude of the tetragonal lattice distortion varies with $R_{V\text{-}V}$. The $AV_2O_4$ path (path 1) and the $Mn_{1-x}Co_xV_2O_4$ (path 2) are indicated by solid and broken lines, respectively.

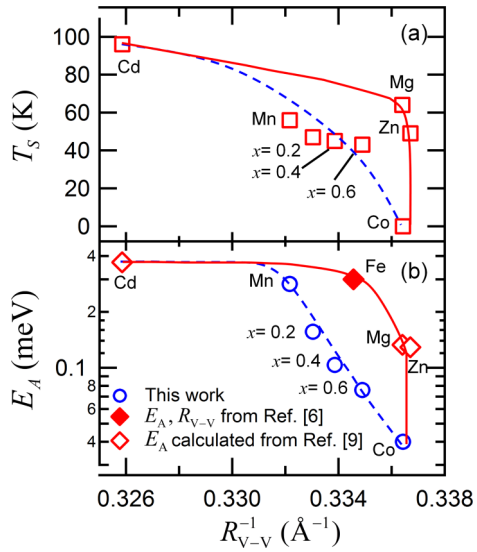


FIG. 6. (Color online) The $R_{V\text{-}V}$ dependencies (plotted as $R_{V\text{-}V}^{-1}$) of (a) the structural transition temperature and (b) the activation energy. The $AV_2O_4$ path (path 1) and the $Mn_{1-x}Co_xV_2O_4$ (path 2) are indicated by solid and broken lines, respectively.

sample with a smaller $R_{V\text{-}V}$. It also indicates that path 2 presents the additional effect of the energy gap between the $A$ site and $V^{3+}$ ions on the itinerancy in addition to the shrinking $R_{V\text{-}V}$.

Following the Co-doping path 2, in $Mn_{1-x}Co_xV_2O_4$, there is an antiferromagnetic $A$-$B$ superexchange interaction via oxygen which is responsible for the ferrimagnetic ordering. A study by Adachi *et al.* demonstrates the magnetic field dependence of $T_S$ in $MnV_2O_4$ where $T_S$ increases with increasing field [21]. This indicates a strong correlation between the magnetic field and $T_S$ where the field stabilizes the tetragonal structure, which in turn also signifies the role of the magnetic $A^{2+}$ cation in spinels. Furthermore, the magnetic structure of $MnV_2O_4$ even turns into a noncollinear two-in-two-out ferrimagnet as temperature decreases. In our case, the substitution with $Co^{2+}$ decreases both the effective moment of the $A$ site and the anisotropy of the system due to the completely filled $e$ orbital, so $T_S$ decreases and the phase separation disappears. This reduction in $T_S$ is also observed in other studies on substitution of $Mn^{2+}$ for a nonmagnetic $A^{2+}$ cation [21,22].

## IV. CONCLUSION

The structural and transport properties of $Mn_{1-x}Co_xV_2O_4$ have been studied and compared to the structural and transport properties of $AV_2O_4$ ($A$ = Cd, Mg, Zn). In approaching the itinerant electron limit, the structural distortion weakens accompanied by vanishing structural transition temperature and decreasing transport activation energy. Even though the nonmagnetic $A$-site ion $AV_2O_4$ and magnetic $A$-site ion $Mn_{1-x}Co_xV_2O_4$ compounds show a qualitatively similar behavior in approaching the electron limit, the $A^{2+}$ ion plays a nonnegligible role in determining the properties in addition of the V-V separation as evident from the two paths that emerge. The difference in the activation energy originates from the projected density of states of V and Co in which the energy difference between the occupied V and Co $d$ states is the smallest, leading to the reduction of the activation energy in the Co-substituted samples which occurs at a larger V-V distance compared to other $AV_2O_4$ samples.

## ACKNOWLEDGMENTS

This work is supported in part by NSF-DMR 1309146 (A.K. and J.S.B.). A portion of this work was performed at the National High Magnetic Field Laboratory, which is supported by the National Science Foundation Cooperative Agreement No. DMR 1157490, the State of Florida, and the U.S. Department of Energy. H.D.Z. acknowledges the support from NSF-DMR through award DMR 1350002. J.M. was sponsored by Scientific User Facilities Division and Office of Basic Energy Sciences, U.S. Department of Energy.

[1] S.-H. Lee, H. Takagi, D. Louca, M. Matsuda, S. Ji, H. Ueda, Y. Ueda, T. Katsufuji, J.-H. Chung, S. Park, S.-W. Cheong, and C. Broholm, J. Phys. Soc. Jpn. **79**, 011004 (2010).

[2] D. B. Rogers, R. J. Arnott, A. Wold, and J. B. Goodenough, J. Phys. Chem. Solids **24**, 347 (1963).

[3] D. B. Rogers, J. B. Goodenough, and A. Wold, J. Appl. Phys. **35**, 1069 (1964).

[4] D. G. Wickham and J. B. Goodenough, Phys. Rev. **115**, 1156 (1959).

[5] S. Blanco-Canosa, F. Rivadulla, V. Pardo, D. Baldomir, J.-S. Zhou, M. García-Hernández, M. A. López-Quintela, J. Rivas, and J. B. Goodenough, Phys. Rev. Lett. **99**, 187201 (2007).

[6] A. Kismarahardja, J. S. Brooks, A. Kiswandhi, K. Matsubayashi, R. Yamanaka, Y. Uwatoko, J. Whalen, T. Siegrist, and H. D. Zhou, Phys. Rev. Lett **106**, 056602 (2011).

[7] R. Kaur, T. Maitra, and T. Nautiyal, J. Phys.: Condens. Matter **26**, 045505 (2014).

[8] A. Kiswandhi, J. S. Brooks, J. Lu, J. Whalen, T. Siegrist, and H. D. Zhou, Phys. Rev. B **84**, 205138 (2011).

[9] V. Pardo, S. Blanco-Canosa, F. Rivadulla, D. I. Khomskii, D. Baldomir, Hua Wu, and J. Rivas, Phys. Rev. Lett. **101**, 256403 (2008).

[10] A. C. Larson and R. B. von Dreele, LANL Report No. LAUR 86-748, 2000 (unpublished).

[11] B. H. Toby, J. Appl. Cryst. **34**, 210 (2001).

[12] N. Nishiguchi and M. Onoda, J. Phys. Condens. Matter **14**, L551 (2002).

[13] H. D. Zhou, J. Lu, and C. R. Wiebe, Phys. Rev. B **76**, 174403 (2007).

[14] M. Reehuis, A. Krimmel, N. Büttgen, A. Loidl, and A. Prokofiev, Eur. Phys. J. B **35**, 311 (2003).

[15] H. Mamiya, M. Onoda, T. Furubayashi, J. Tang, and I. Nakatani, J. Appl. Phys. **81**, 5289 (1997).

[16] A. N. Vasiliev, M. M. Markina, M. Isobe, and Y. Ueda, J. Magn. Magn. Mater. **300**, e375 (2006).
[17] A. T. M. Nazmul Islam, E. M. Wheeler, M. Reehuis, K. Siemensmeyer, M. Tovar, B. Klemke, K. Kiefer, A. H. Hill, and B. Lake, Phys. Rev. B **85**, 024203 (2012).
[18] Z. Zhang, D. Louca, A. Visinoiu, S.-H. Lee, J. D. Thompson, T. Proffen, A. Llobet, Y. Qiu, S. Park, and Y. Ueda, Phys. Rev. B **74**, 014108 (2006).
[19] J. Ma, J. H. Lee, S. E. Hahn, Tao Hong, H. B. Cao, A. A. Aczel, Z. L. Dun, M. B. Stone, W. Tian, Y. Qiu, J. R. D. Copley, H. D. Zhou, R. S. Fishman, and M. Matsuda, arXiv:1407.4143.
[20] S. Sarkar and T. Saha-Dasgupta, Phys. Rev. B **84**, 235112 (2011).
[21] K. Adachi, T. Suzuki, K. Kato, K. Osaka, M. Takata, and T. Katsufuji, Phys. Rev. Lett. **95**, 197202 (2005).
[22] Y. Huang, Z. Qu, and Y. Zhang, J. Magn. Magn. Mater. **323**, 975 (2011).